Science of the Total Environment 886 (2023) 163923

Contents lists available at ScienceDirect

Science of the Total Environment

journal homepage: www.elsevier.com/locate/scitotenv

# A green approach of biochar-supported magnetic nanocomposites from white tea waste: Production, characterization and plausible synthesis mechanisms

Na Zhang [a], Febelyn Reguyal [a], Sai Praneeth [b], Ajit K. Sarmah [a,c,*]

[a] Department of Civil & Environmental Engineering, The Faculty of Engineering, The University of Auckland, Private Bag 92019, Auckland 1142, New Zealand
[b] Department of Civil & Environmental Engineering, Wayne State University, Detroit, MI 48202, USA
[c] The Institute of Agriculture, University of Western Australia, 35 Stirling Highway Perth, WA 6009, Australia

## HIGHLIGHTS

- $Fe_3O_4$-biochar nanocomposites (GSMB) were prepared from white tea waste via green synthesis.
- GSMB exhibited superior morphological and functionalization properties than other magnetic biochars.
- GSMB showed a saturation magnetization value of 11.5 $Am^2/kg$.
- GSMB exhibited excellent $Pb^{2+}$ and $Cd^{2+}$ adsorption removal capacity from water.

## GRAPHICAL ABSTRACT

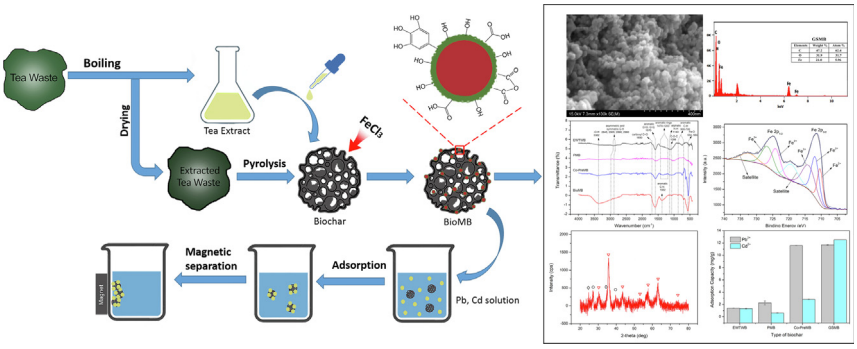


## ARTICLE INFO

Editor: Damia Barcelo

*Keywords:*
Green synthesis
Magnetic biochar
Nanoparticles
Tea waste
$Fe_3O_4$

## ABSTRACT

Green synthesized magnetic nanoparticles were impregnated into biochar matrix (EWTWB) to produce biochar-supported magnetic nanocomposite (GSMB). Instead of chemicals, organic matters in white tea waste extract were used as reductant, surfactant and functional capping materials. Magnetic biochar produced from traditional methods of pyrolysis (PMB) and co-precipitation (Co-PreMB) were prepared to compare their properties with GSMB. Xray Diffraction confirmed the main component of green synthesized particles is $Fe_3O_4$. When compared with PMB and Co-PreMB, the $Fe_3O_4$ produced by co-precipitation method has higher purity while the products from green synthesis method are complex and contain a small portion of other iron-containing compounds. As a consequence, Co-PreMB has higher saturation magnetisation value than GSMB, which are 31.3 and 11.5 $Am^2/kg$, respectively. GSMB was also found to be less stable in acidic conditions (pH ≤ 4) than Co-PreMB. However, the SEM results exhibited that spherical magnetic nanoparticles (20–50 nm) were successfully formed and distributed on the surface of biochar via green synthesis method while serious aggregation occurred on the surface of Co-PreMB. According to the result of BET, the surface area of GSMB increased dramatically from 0.2 $m^2/g$ to 59.7 $m^2/g$. Fourier Transform Infrared spectroscopy and Xray photoelectron spectroscopy results showed the presence of rich oxygen-containing functional groups on the GSMB, The high surface area coupled with rich functional groups on the GSMB made the whole synthesis process an environmentally friendly and greener, to prepare magnetic biochar for application in wastewater treatment.

* Corresponding author at: Department of Civil and Environmental Engineering, The Faculty of Engineering, The University of Auckland, Private Bag 92019, Auckland 1142, New Zealand.
*E-mail address:* a.sarmah@auckland.ac.nz (A.K. Sarmah).

http://dx.doi.org/10.1016/j.scitotenv.2023.163923
Received 12 February 2023; Received in revised form 6 April 2023; Accepted 29 April 2023
Available online 6 May 2023

## 1. Introduction

Biochar, a biomass derived carbonaceous solid material produced via thermochemical conversion in the absence or under limited amount of oxygen has emerged as one of the most promising adsorbents. However, due to the small size of biochar, it is difficult to recover it after its use in aqueous solution (Yao et al., 2020). To improve its separation ability from aqueous solution, biochar has been magnetized using iron/iron oxides, including zero-valent iron (ZVI), magnetite ($Fe_3O_4$) and maghemite ($\gamma$-$Fe_2O_3$) (Qiu et al., 2020). These iron/iron oxide materials themselves are also promising alternatives for wastewater treatment, and their ability to remove contaminants has been demonstrated at both laboratory and field-scale (Nassar et al., 2014; Mohammadian et al., 2021). However, owing to the high surface energy arising from strong Van der Waals forces, the iron/iron oxide nanoparticles (especially magnetite) tend to aggregate in aqueous solutions, which dramatically decrease the surface area and adsorption abilities as well as increase the cost (Nassar et al., 2014). To overcome the problem, many solid supporting materials have been applied (Khan et al., 2020) where biochar has been emerged as a popular mechanical support to disperse and stabilize engineered nanoparticles (NPs) to facilitate their environmental application (Tan et al., 2016). Therefore, the integration of iron/iron oxide nanoparticles (Fe/FeONPs) with biochar is not only a win-win approach that can combine the advantages of both but also overcome the drawbacks of each other.

In general, pyrolysis of iron-pre-treated biomass and chemical co-precipitation of biochar iron solution are the two main methods for introducing magnetic particles onto biochar (Tan et al., 2016). Pyrolysis method combines iron oxide particles formation with biochar preparation into one-step, which activation and magnetization simultaneous occur during pyrolysis. However, the operation of pyrolysis method is difficult to control which may result in low conversion rate and consequently low magnetic capacity of the adsorbents. Co-precipitation combines mixing and heating and does not require special equipment. However, the co-precipitation method easily aggregates the adsorbents and surfactants need to be added to prevent the aggregation. The use of surfactants increases the operational cost and leads to secondary pollution. Therefore, there is an urgent need to find more effective and 'cleaner' strategy to introduce magnetic particles onto biochar such as green synthesis.

Green synthesis uses natural resources (plants extract, algae, bacteria, etc.) is viewed as not only environmentally friendly due to non-involvement of hazardous solvents or other toxic ingredients, but also inexpensive (Mondal et al., 2020), as it does not require high temperature, pressure, or additional energy input. NPs produced using green synthesis are generally biocompatible and have functional surface, making the combination of NPs with biochar even more promising in wastewater treatment. And there have been some studies applying green synthesis method to produce iron-containing biochar composites (Table S1), however, green synthesis has never been used for introducing magnetic NPs onto biochar until now.

Among many bioresources, plant-based materials seem to be the best candidates and they are more suitable for large-scale 'green synthesis' of NPs (Makarov et al., 2014). Therein, tea leaves, which are rich in active polyphenols and caffeine, has emerged as the most suitable material for green synthesizing metal NPs. Polyphenols are powerful antioxidants and free radical scavengers, it can reduce iron precursors into different phases of iron oxides and oxyhydroxides (Table S2). Meanwhile, the organic compounds present in tea extract can also prevent the NPs from aggregating as well as functionalize the particles for the desired applications at the same time.

The current studies on synthesizing iron-containing NPs via tea extract mainly used unbrewed tea leaves rather than tea waste/tea residue, as unbrewed tea contains more active agent for reduction than the brewed tea, and only a few studies studied green synthesis via tea waste/residue (Table S2). Actually, the tea without brewing can be more efficient in synthesizing iron-containing NPs, however, it lost its economic applicability in practical production due to the high economic value of tea leaves. Meanwhile, with the rapid increase in global tea consumption, enormous quantities of tea wastes were produced every year in the worldwide (Guo et al., 2021). Around the world, the production of tea amounted to 5.73 million tonnes in 2016. In Turkey, approximately 30,000 t of waste generated by tea factories are disposed of each year in the small bays close to the Black Sea, which has the potential to cause pollution to the air, soil, and water. Therefore, more efforts should be put into developing tea waste as biomass for green synthesis. White tea is known to be one of the most delicate tea varieties which undergoes minimal processing (only drying after picking to prevent oxidation), keeping the white tea a rich source of polyphenols which waste could also be a good candidate for synthesizing Fe/FeONPs. Additionally, the tea waste after extracting is still pose hazardous potential to the environment, as the watery tea residue is prone to rot if not treated in time. The most common way to deal with tea waste is to burn or bury locally at present, as added value of these methods are far more less than the amount spent in its production and most of the tea waste were discarded without any processing (Chowdhury et al., 2016). Therefore, more efficient application of tea waste are demanding, and accordingly converting tea waste biomass into biochar could be an effective alternative strategy (Guo et al., 2021).

The overarching objective of this study is to propose a green synthesis method to prepare magnetic biochar using white tea waste extract to impregnate magnetic NPs into extracted white tea waste biochar (EWTWB). Pyrolysis and co-precipitation methods were also applied to produce magnetic biochar (PMB and Co-PreMB) to compare with the green synthesis method produced biochar-based magnetic nanocomposites (GSMB). Arrays of characterization techniques were used for physical and chemical properties determination of the magnetic biochars.

## 2. Materials and methods

### 2.1. Materials

White tea was obtained from Tianmu Lake (Jiangsu, China) and white tea waste was collected after the tea was brewed in hot water. White tea waste extract was obtained by boiling the tea waste in Milli-Q water for 30 min, the residue (exhausted white tea waste) was dried and ground to pass 100-mesh sieve for further application. Exhausted white tea waste biochar (EWTWB) was produced from exhausted white tea waste by slow pyrolysis at 450 °C and was washed three times with Milli-Q water then oven-dried at 105 °C overnight. Following this, EWTWB was ground to pass through a 100-mesh sieve prior to its application in the synthesis process.

The chemicals: ferric chloride ($FeCl_3$, 98 %), ferrous sulfate ($FeSO_4$, 98 %), polyethylene glycol (PEG), sodium hydroxide (NaOH, 98 %), hydrochloric acid (HCl), nitric acid (HNO3) were all analytical grade and purchased from Sigma-Aldrich and used as received. The $N_2$ gas used in the synthesis was purchased from BOC, New Zealand.

### 2.2. Preparation of green synthesized magnetic biochar

The green synthesis of magnetic biochar was carried out following modification of Li and Yang (2016). Briefly, 1.0 g EWTWB was added into 90 mL 0.1 M $FeCl_3$ solution, stirred for 30 min (under $N_2$), the mixture was heated to 80 °C and 90 mL 10 g/L white tea waste extract was added dropwise. During this process, 1 M NaOH solution was slowly added to adjust the pH to 10 and the pH was maintained for another 30 min after the addition of tea extract. The green synthesized modified biochar (GSMB) was obtained by centrifugation, washed three times with Milli-Q water until the pH of eluate reached neutral before oven-dried at 105 °C overnight. Then GSMB was sieved (100-mesh) and stored in a sealed container for further studies. The detail information regarding the preparation of PMB and Co-PreMB was presented in the supplementary information (Text S1 and Text S2).

### 2.3. Characterization

The elemental compositions (C, H and N) of EWTWB, PMB, Co-PreMB and GSMB were measured at the Campbell Microanalytical Laboratory, New Zealand. Iron content of each biochar was measured using Microwave Digestion System (Ethos One, Milestone, Italy). Micromeritics Tristar 3000 instrument was used in $N_2$ gas adsorption/desorption isotherm test under liquid nitrogen (−196 °C). From adsorption/desorption isotherm data, specific surface areas, and cumulative pore volume and pore diameter were determined according to the Brunauer-Emmett-Teller (BET) and Barrett-Joyner-Halenda (BJH) methods, respectively. Prior to the $N_2$ adsorption, samples were degassed for overnight at 300 °C under $N_2$ gas. The Zeta potential of each biochar was determined by placing a 0.002 g sample in 25 mL Milli-Q water. The suspension pH was adjusted within the range of 2–9, using 0.1 M NaOH and 0.1 M HCl. The suspensions were ultrasonically dispersed in a bath-type sonicator for 3 h at 25 °C. The electrophoresis mobility was measured using the JS94G + micro electrophoresis apparatus (Zetasizer Nano ZS90, Malvern, UK). The magnetic property was measured at external magnetic fields ranging between ± 7.16 MA/m using physical property measurement system (PPMS) under vibrating sample magnetometer (VSM) option.

Surface morphology and iron distribution on the surface were visualized and determined using Scanning Electron Microscopy-Energy Dispersive X-ray Spectroscopy (SEM-EDX, Thermo Scientific, SU-70, US). To identify the crystalline structure of the magnetic biochar, X-Ray Diffraction (XRD, Ultima IV, Rigaku, Japan) with CuKα radiation (λ = 5406 Å) was performed. Data were recorded over 2θ range of 20–80 with a step increment of 0.02 and interval time of 0.008 s per step. Fourier Transform Infrared Spectroscopy (FT-IR, INVENIO R, Bruker, Germany) was performed to determine the surface functional groups of each biochar. Composition and speciation of surface elements were identified using X-ray Photoelectron Spectroscopy (Kratos Axis Ultra DLD X-ray Photoelectron Spectrometer, Kratos Analytical, Manchester, United Kingdom) equipped with hemispherical electron energy analyser. The spectra were excited using monochromatic Al Kα X-rays (1486.69 eV0 with the X-ray source operating at 150 W. CasaXPS software was used for data analysis while Shirley backgrounds were used in peak fitting.

### 2.4. Stability of magnetic biochar prepared

Leaching tests were carried out to determine the stability of iron component in each adsorbent at different pH. The details of leaching test were present in Text S3, and the determine of pH range was presented in Text S4 and Fig. S1. After leaching, the samples were filtered by 0.22 $\mu m$ regenerated cellulose membrane and acidified by concentrated $HNO_3$. Following this, the filtrate was analyzed using Microwave Plasma-Atomic Emission Spectroscopy (MP-AES, Agilent Technologies, 4210, US) to measure iron concentration at 371.99 nm wavelength.

## 3. Results and discussion

### 3.1. Properties of synthesized adsorbents

Some of the physicochemical properties of EWTWB, PMB, Co-PreMB, and GSMB are summarized in Table 1. The lowest H/C and O/C value of PMB can be explained by the loss of organic residues in high pyrolysis temperature (Pariyar et al., 2020). GSMB possessed a higher H/C value to EWTWB and PMB, and the highest O/C among all the adsorbents prepared, indicating the biochar was successfully capped by the organic compounds from tea extract. Additionally, the high O/C of GSMB also suggest a strong affinity to water, allowing water to diffuse into its solid regions and lead to some swelling. Therefore, adsorption in GMSB might occur below the surface or even throughout substantial portions of the solid regions (Essandoh et al., 2017). The iron content measured in EWTWB is negligible. Comparably, PMB, Co-PreMB and GSMB contain 3.61 %, 27.0 % and 30.3 % of Fe respectively, indicative of the successful impregnation of iron into biochar by all the three methods, and co-precipitation and green synthesis are much more effective than the pyrolysis method in this study.

**Table 1**
Physical-chemical properties of synthesized adsorbents.

| Properties | Adsorbents | | | |
|---|---|---|---|---|
| | EWTWB | PMB | Co-PreMB | GSMB |
| C (%) | 69.9 | 74.7 | 43.2 | 38.26 |
| H (%) | 3.36 | 1.69 | 2.72 | 2.115 |
| N (%) | 6.04 | 7.55 | 5.13 | 3.22 |
| Fe (%) | n.d | 3.61 | 27.0 | 30.3 |
| $Fe_3O_4$[a] (%) | n.d | 4.99 | 37.4 | 41.8 |
| O[b] (%) | 20.7 | 11.1 | 11.6 | 14.605 |
| Molar H/C | 0.577 | 0.271 | 0.756 | 0.663 |
| Molar O/C | 0.222 | 0.111 | 0.201 | 0.286 |
| $S_{BET}$[c] ($m^2$/g) | 0.196 | 36.6 | 32.8 | 52.2 |
| APD (nm) | 27.7 | 13.5 | 14.4 | 9.07 |
| TPV[c] ($cm^3$/g) | 0.0006 | 0.0123 | 0.146 | 0.118 |
| Ms[d] ($Am^2$/kg) | n.d. | 0.05 | 31.3 | 11.5 |

[a] Assumption: All total iron have completely formed into $Fe_3O_4$.
[b] %O was obtained by mass difference $(100 - \%C - \%H - \%N - \%Fe_3O_4)$.
[c] $N_2$ isotherm at −196 °C; $S_{BET}$ (BET Surface Area); APD (Average Pore Diameter); TPV (Total Pore Volume).
[d] Magnetisation saturation value.

A recent study by Wan et al. (2020) found that the addition of Fe may block the pore structure of biochar and resulted in reduction of surface area. On the contrary, the surface area and porosity developed markedly for all the three modified biochars in this study. This could be due to the removal of the high tarry components in EWTWB at high temperature or reaction with alkali hydroxides that formed water-soluble salts and removed during NaOH treatment, leading to the enhancement of porosity (Mohan et al., 2014). Additionally, the improvement of porosity may be partially a result of the reduction of the organic content in the biochar during the formation of iron oxide/biochar hybrid particles (Mohan et al., 2014).

The surface charge of biochars was measured as zeta potential and presented in Fig. S2. It can be observed that the point of zero charge of EWTWB, PMB, Co-PreMB and GSMB were 3.2, 2.2, 3.9 and 3.7, respectively. The higher $pH_{PZC}$ value of Co-PreMB and GSMB than EWTWB can be explained by the impregnation of $Fe_3O_4$, which has a $pH_{PZC}$ value of 6 (Wang et al., 2010). Normally, biochar produced at higher temperature carried less negative charges due to lack of acidic functional groups (Yuan et al., 2011). However, the PMB in this study possessed the lowest point of zero charge which could be attributed to low content of iron composites. Given the same pH conditions, PMB carried the most negative surface charges and possessed the highest electrostatic adsorption potential in the range of pH 2–9, followed by GSMB and Co-PreMB (Xu et al., 2019).

Among the adsorbents, PMB (134.5 μm) has the smallest particle size due to its high pyrolysis temperature while larger particles were observed for Co-PreMB (213.9 μm) and GSMB (139.2 μm) due to the iron impregnation. However, as compared to Co-PreMB, GSMB exhibited a smaller particle size even though it impregnated more iron than Co-preMB. The organic molecules in tea extract can be effective in inhibiting aggregation which contribute to a better distribution of iron particles on the surface of biochar and lead to a minor particle size increase of GSMB (Wang et al., 2014). The iron-containing particles were not only very easy to accumulate on the surface of biochar but may also cause an aggregation between biochars, resulting in a big increase in particle size of Co-PreMB.

On the other hand, the magnetic properties of three modified biochar were studied using VSM at 300 K. The saturation magnetisation ($M_s$) values were 31.3 and 11.5 $Am^2$/kg for Co-PreMB and GSMB, respectively. The PMB displayed *Ms* value of only 0.05 $Am^2$/kg, which was not consistent with the previous results (Zhang et al., 2013; Yang et al., 2016) and confirmed the failure of preparing magnetic biochar by pyrolysis method in this study. Additionally, the lower value of GSMB than Co-PreMB may be due to the impurity of $Fe_3O_4$ and the diamagnetic properties of the

biomolecule coating material surround the nanoparticles (Vinayagam et al., 2021), or the crystalline defect and alignment of the magnetic moment in nanocrystals.

### 3.2. Surface morphology analysis

As shown in Fig. 1, SEM images depicting surface morphological characteristics of different biochars, and the bright spots in SEM provide an indication that some degree of conductivity exists with the presence of iron-containing particles in this study (Mohan et al., 2014). As shown in Fig. 1A (1–3), the surface of EWTWB was highly porous due to volatile matter elimination, resulting in the formation of pores with an average pore diameter at 27.7 nm. The original morphology of plant cell structure was still visible in EWTWB after pyrolysis and its surface was smoother than the companion magnetic biochar.

In contrast, the surface of Co-PreMB and GSMB were coated with bright spots and some pores were blocked (Fig. 1C, D), leading to lower pore diameters of 14.4 and 7.7 nm, respectively (Table 1). The images C2 and D2 clearly showed the deposition of iron-containing particles on the biochar surface. Compared to Co-PreMB, the surface of GSMB was rougher, as the distribution of iron composites introduced into biochar by green synthesis method were more separated even though aggregation still occurred. The composites introduced by co-precipitation method demonstrated strong aggregation and formed into a densified shell with different size of particles embedded on the surface of biochar. Additionally, the iron-containing particles in GSMB (Fig. 1D4) were uniform in shape and size with a diameter at around 20–50 nm, indicating the success of introducing nanoparticles into biochar by green synthesis method. The particles impregnated in Co-PreMB were in a wide range from nano-size to micro-size due to the aggregation, which may explain why Co-PreMB possessed a smaller surface area than GSMB. However, according to the Fig. 1C3, the particles in Co-PreMB were partly embedded in the biochar, indicating a strong mechanical interlocking between the introduced particles and biochar, which prevents the separation of the particles from biochar matrix when exposed to external forces caused by water. Comparatively, the nanoparticles in GSMB were only bound onto the surface of the biochar which has a high risk of particle loss and contamination of the solution during adsorption process.

PMB possesses a rougher surface than the pristine biochar due to the higher pyrolysis temperature, and no obvious particle substance were observed (Fig. 1B3). Combined with the result from digestion in Table 1, pyrolysis method in this study was far less effective than the other two methods in magnetic biochar production. As mentioned above, the operational conditions of pyrolysis method used for magnetic biochar preparation in the current work is rather difficult to control, even though the condition used in this study performed very well in other studies (Zhang et al., 2013; Yang et al., 2016), it is not suitable in this study.

Fig. 1 (A2, B2) shows some bright spots were also visible on the surface of EWTWB and PMB. To further confirm the successful impregnation of iron-containing particles EDX (Fig. 2) was conducted, and the area selected for EDX analysis were all bright spots (red area/dots shown in Fig. 1) which were estimated to be iron-containing particles. EDX result of the highlighted area on the surface of EWTWB did not, however, exhibit any Fe peaks, albeit a small one in PMB. In contrast, on the surface of Co-preMB and GSMB, intense Fe peaks could be observed confirming the iron loading in Co-PreMB and GSMB.

However, as shown in Fig. 2, the iron content of Co-PreMB is higher than GSMB, which is opposite to the result obtained from digestion (Table 1) EDX can only measure surface elemental content of samples, hence, GSMB had lower Fe content on the surface due to capping by polyphenols in tea extract (Huang et al., 2014). Additionally, O content in Co-PreMB and GSMB is much higher than the pristine biochar, indicating the iron-containing particle introduced by co-precipitation and green synthesis method might be iron oxides. The higher rate of O/Fe in GSMB than Co-PreMB can be contributed by the organic compounds coated on the surface of the iron-containing NPs in GSMB (Kheshtzar et al., 2019). However, the O content in PMB particle is nil, which might be attributed in part to side reactions that could convert $Fe^{3+}$ to $Fe^{o}$ or/and $Fe_3C$.

### 3.3. Fourier Transform Infrared (FTIR) analysis

FTIR analysis was employed to compare the differences in surface functionality of magnetic biochar produced by different methods. FTIR analyses enable the evaluation of the possible biomolecules responsible for the reduction of the $Fe^{3+}$ in the green synthesis method (Shahwan et al., 2011). As shown in Fig. 3, it is obvious that the magnetic biochar produced from pyrolysis method (PMB) exhibited least functional groups compared to the EWTWB and the other two magnetic biochars. There was no Fe—O band detected in PMB, confirming the unsuccessful formation of iron oxides by pyrolysis method. Strong absorption peaks at 554 and 564 $cm^{-1}$ were ascribed to the Fe—O vibration from the magnetite phase that appeared in Co-PreMB and GSMB respectively, confirming the successful formation of iron oxides (Lin et al., 2017). And it is obvious that Fe—O stretching is the dominant bond in Co-PreMB which is sharp and strong while GSMB showed many other functional bonds even though it contains more iron (Table 1), indicating the functionality of GSMB.

Broad peaks at 3020–3640 $cm^{-1}$ were attributed to the presence of -OH stretching vibration. The weak -OH band in Co-PreMB could be due to water molecular (Hui and Salimi, 2020), and the intense -OH band in GSMB was mainly contributed by the biomolecules in tea extract. In EWTWB, the two absorption bands at 2845, and 2905 $cm^{-1}$ are ascribed to the asymmetric and symmetric C—H stretching, respectively (Shen et al., 2009), while in the other three modified biochars the two C—H bands shifted to 2890 and 2980 $cm^{-1}$ (Mahdavi et al., 2013). The small peak at around 1690 $cm^{-1}$ in EWTWB and Co-PreMB were due to the carbonyl C═O stretching vibration, and the peaks at approximately 1570 $cm^{-1}$ in all the biochars were related to C═O and C═C stretching of aromatic rings (Pal and Maiti, 2019). The disappearance of carbonyl C═O in GSMB may be attributed to the overlap of its aromatic C═O and C═C stretching band, whose intensity is much stronger than other prepared adsorbents. The presence of new band appeared at 1362 $cm^{-1}$ corresponded to C—N stretching vibration for aromatic amines (Wang et al., 2014). The intense -OH band, aromatic C═O and C═C band, and the presence of new C—N band in GSMB confirmed the successful coating of some oxidized polyphenols on the surface of GSMB. However, the broad C-O-C stretching band at 1098 $cm^{-1}$ and N—H stretching vibration of aliphatic amines at 1140 $cm^{-1}$ in EWTWB almost disappear after modification, the reduction in PMB was caused by the high pyrolysis temperature while the loss of some volatile matters in alkali condition may explain the band decreases in Co-PreMB and GSMB. Many spectral bands in the region between 1470 and 1200 $cm^{-1}$ were attributable to in-plane skeletal vibrations in aromatic rings with bands appearing in the range of 900–700 $cm^{-1}$ were due to out of plane deformation of aromatic C—H (Rajapaksha et al., 2014).

### 3.4. X-ray Photoelectron Spectroscopy (XPS) analysis

XPS was used to determine the elemental composition and oxidation state of the magnetic nanocomposites. Fig. S3 shows the overall XPS spectrum of the pristine biochar, and three magnetic biochars produced from different methods. C1s and O1s bonds were found in all the tested biochars, proving the presence of carbon and oxygen. In the spectrum of Co-PreMB and GSMB, distinct Fe($3p_{3/2}$), Fe($2p_{3/2}$) and Fe($2p_{1/2}$) bonds at about 55, 710 and 724 eV were detected, which are due to Fe—O bond of the $Fe_3O_4$ nanoparticles (Maity et al., 2009). The spectrum of PMB did not show obvious Fe bonds which may be due to the low content of iron (At.% = 1.66), consistent with previous elemental analysis and EDX results. The table in Fig. S4 shows that the atomic percentage of C decreased heavily while the O% increased greatly after iron impregnation in Co-PreMB and GSMB. The result of lower O and Fe but higher C

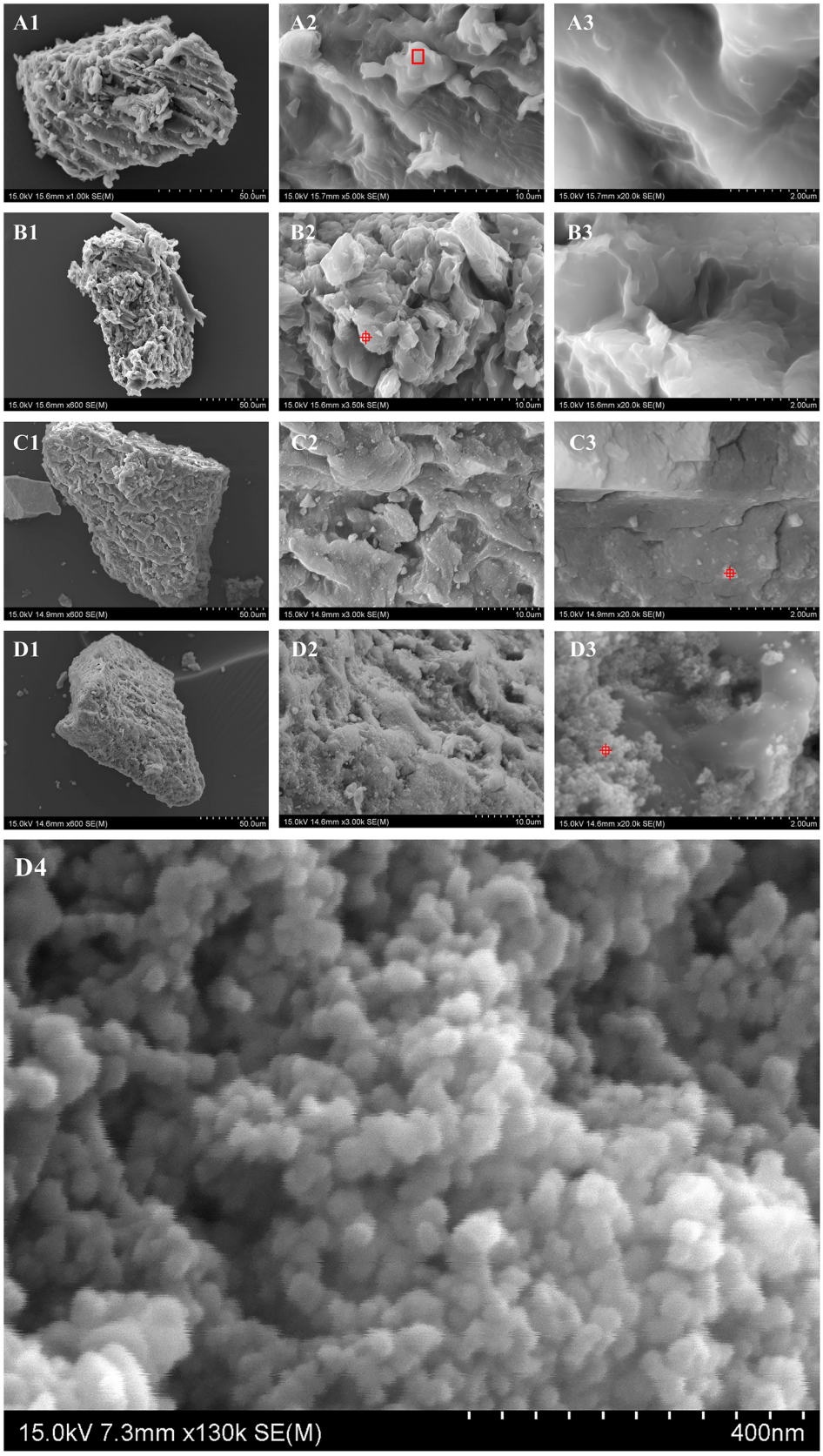


**Fig. 1.** SEM micrographs of EWTWB (A), PMB (B), Co-PreMB (C) and GSMB (D) at different magnifications.

content on the surface of GSMB than Co-PreMB is consistent with the EDX result which is due to the capping of organic matters from tea extract onto iron oxides nanoparticles.

Fig. 4 show the C1s, O1s and Fe2p XPS spectra of each biochar. As can be seen in Fig. 4a and Table S3, the C1s spectrum of EWTWB were deconvoluted into five major peaks corresponding to carbide (281.6 eV),

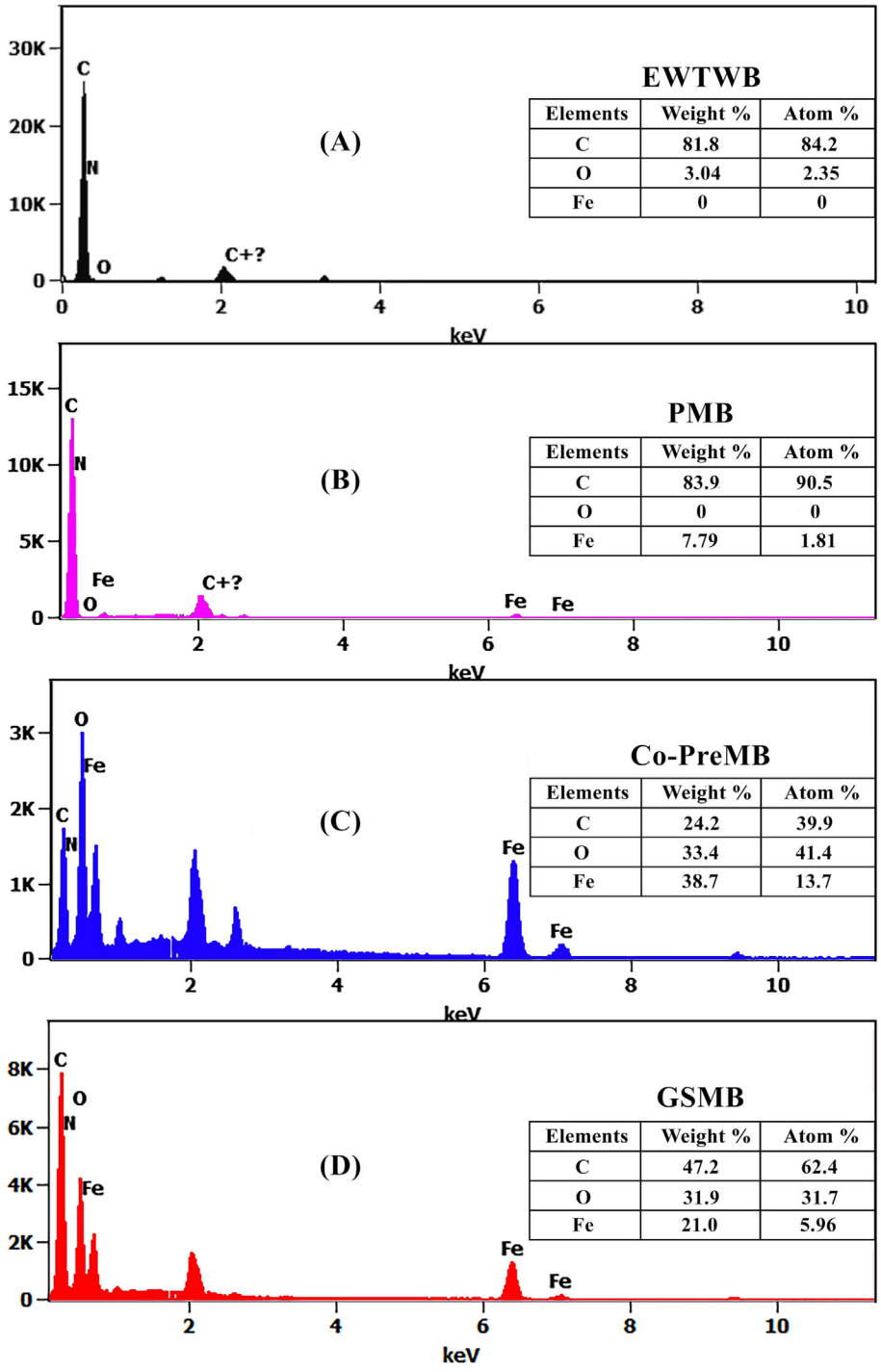


**Fig. 2.** EDX results of EWTWB (A), PMB (B), Co-PreMB (C) and GSMB (D).

C—H (282.7 eV), C-C/C=C (284.3 eV), C-O-C (285.5 eV) and C=O (287.8 eV) (Hu et al., 2015). After magnetization by different methods, the C1s components of biochars varied differently. The carbide and C—H bond in C1s spectrum of PMB is diminished due to the pre-treatment and the high pyrolysis temperature process during the modification. The peaks around 281 eV in the C1s spectrum of Co-PreMB and GSMB were assigned to carbide which intensity enhanced dramatically after the successful impregnation of iron oxide by co-precipitation and green synthesis method (Reguyal and Sarmah, 2018). XPS spectra, associated with elemental analysis and FTIR analysis, confirms the presence of different functional groups on Co-PreMB and GSMB surface. As compared with Co-PreMB, a new peak corresponding to C—N (286.2 eV) appeared in the C1s spectrum of GSMB (Zhao et al., 2019), and the proportion of oxygen-containing functional groups in GSMB is higher, confirming the surface functionalisation of green synthesis method.

The binding energy in the O1s region between 528.6 eV and 529.9 eV can be attributed to metal oxides in biochars. In EWTWB, the metal oxides could be $K_2O$, CaO, MgO etc. (Chen et al., 2022), and these contents were washed out during the pre-treatment of PMB (Table S2). In Co-PreMB and GSMB, the bonds are mainly inorganic oxygen bonded to iron (FeO, $Fe_2O_3$, $Fe_3O_4$ or FeOOH) due to the large amount of Fe introduced (Reguyal and Sarmah, 2018). However, PMB did not show obvious Fe—O bond in the O1s spectrum even if it contains a certain amount of iron. There are three possible explanations for this result: 1) the iron

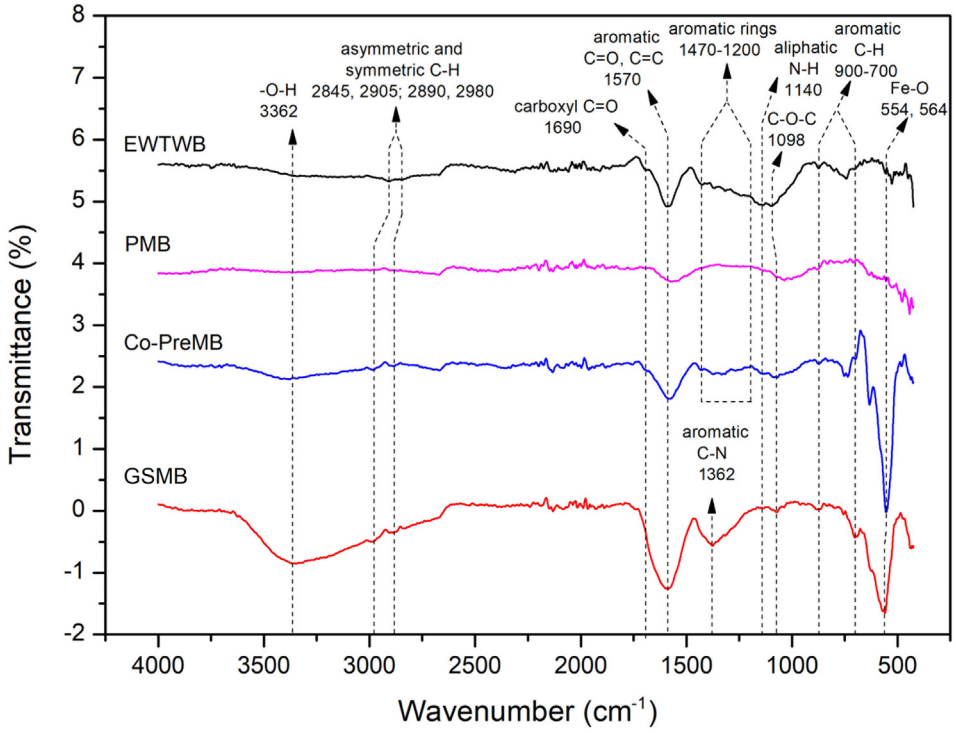


**Fig. 3.** FT-IR spectra of prepared adsorbents obtained under different modification methods.

particles produced according to the pyrolysis is ZVI (Liu et al., 2019), 2) other forms of iron composites which iron did not bond to oxygen produced (Yang et al., 2016), or 3) the peak of Fe—O in PMB is too weak that was overlapped by next strong broad peak. The newly appearing peak at 531 eV in Co-PreMB and GSMB were attributed to -OH, which mainly came from moisture and polyphenols coated, respectively, consisting with the results of FTIR.

In the deconvoluted Fe2p spectrum of Co-PreMB and GSMB, seven peaks were observed. The three spectral bands located at 712.7/711.9 eV, 714.5/713.9 eV and 727.1/727.9 eV were corresponded to $2p_{1/2}$, $2p_{3/2}$ of $Fe^{3+}$ species, respectively. And the other two peaks at binding energy of 710.7/710.3 eV and 724.7/723.6 eV could be attributed to $2p_{1/2}$ and $2p_{3/2}$ of $Fe^{2+}$ species. Combine with the remaining two peaks at 719.9/719.3 eV and 733.1/732.4 eV which were corresponding satellite peaks of $Fe^{3+}$ and $Fe^{2+}$, indicating the successful formation of the $Fe_3O_4$ phase in both Co-PreMB and GSMB (Reddy et al., 2018). Since stoichiometric $Fe_3O_4$ can also be expressed as $FeO{\cdot}Fe_2O_3$, where the $Fe^{2+}/Fe^{3+}$ ratio should be ½ (Yamashita and Hayes, 2008). In this study, the results of $Fe^{2+}/Fe^{3+}$ according to the deconvoluted peaks of Co-PreMB and GSMB are 0.499 and 0.567 respectively, indicating the purity of $Fe_3O_4$ produced by co-precipitation method while the $Fe_3O_4$ nanoparticles produced by green synthesis were a mixture of iron-containing materials. The weak peak of $Fe^0$ (707.4 eV) (Wei et al., 2017) in the Fe2p spectrum of PMB supports the potential formation of ZVI, however, the content of ZVI is quite small (At.% = 2.4 %), the rest of iron were presented in the form of $Fe_3C$ or $FeCl_2$ due to the side reaction of pyrolysis method which indicated by the two distinct peaks of Fe $2p_{3/2}$ (711.1 eV) and Fe $2p_{1/2}$ (724.4 eV) in Fig. 4i (Huang et al., 2018), and the absence of Fe—C (carbide) in the C1s spectrum could be due to its insufficient amount (Wei et al., 2017).

### 3.5. X-ray Diffraction (XRD) analysis

To further confirm the species of iron containing particles introduced into biochar, XRD analysis for PMB, Co-PreMB and GSMB was conducted as shown in Fig. 5. It can be observed that no distinctive peaks were present on the spectra of PMB (Fig. 5A), indicating the PMB was not crystalline in nature and possessed amorphous structure. The result obtained may be explained by the significantly low iron levels observed, which is in line with earlier outcomes. In comparison, multiple sharp phase peaks were observed in the 2θ range of 20–80° for both Co-PreMB and GSMB (Fig. 5B, C), implying the degree of crystallinity in phases present in the two biochars. Peaks were keen edged at 30.5°, 35.8°, 43.4°, 54.0°, 57.5°, 63.1°, 71.6° and 74.6° in Co-PreMB were coincident with the phase of $Fe_3O_4$ (JCPDS, PDF Number 01–071-6336). The weak diffraction peak at 26.6° as observed could be attributed to amorphous carbon (Yang et al., 2016). No other peaks are observed in Fig. 5, indicating that the iron-containing particles, impregnated via co-precipitation method, are primarily composed of $Fe_3O_4$.

The strong and sharp peaks of $Fe_3O_4$ located at approximately 30.5°, 35.7°, 43.5°, 53.9°, 57.2°, 63.1° and 74.1° in Fig. 5C suggest that the $Fe_3O_4$ is also highly crystalline in GSMB (JCPDS, PDF Number 01-071-6336). However, there are some other peaks observed in GSMB, at 27.2°, 39.7° and 47.0° which were assigned to β-FeOOH (JCPDS PDF Number 34-1266), and the peak at 24.6°, 34. 6° are assigned to α-$Fe_2O_3$ (JCPDS PDF Number 01-085-0599). The peaks related to β-FeOOH and α-$Fe_2O_3$ are evidently less pronounced and weaker than those attributed to $Fe_3O_4$, indicating that $Fe_3O_4$ constitutes the primary component of the green-synthesized nanoparticles. The impurity of iron oxides in GSMB is consistent with previous findings and can be explained by many phytochemicals in tea extracts, which can reduce iron precursors into different phases, resulting in many different kinds of iron-containing NPs such as zero-valent iron, iron hydroxides and iron complex (Table S2). As observed, the iron oxides generated through the green synthesis method could potentially have an amorphous structure, accounting for the lower crystallinity of GSMB compared to Co-PreMB. Furthermore, the presence of bioorganic molecules on the NPs' surface, which lead to noise signals in the spectra of GSMB, may also contribute to the less crystalline structure observed (Parvathy et al., 2021). According to Scherrer's formula, the average crystallite size was determined to be 8.78 nm, which is notably smaller than the size range of 20–50 nm observed in the SEM images. This discrepancy may be attributed to the thick coating layer present on the surface of the nanoparticles, which is visible in SEM but not considered during the XRD crystallite size calculation. Additionally, the significant noise present in the XRD spectra may also have affected the accuracy of the crystallite size calculation.

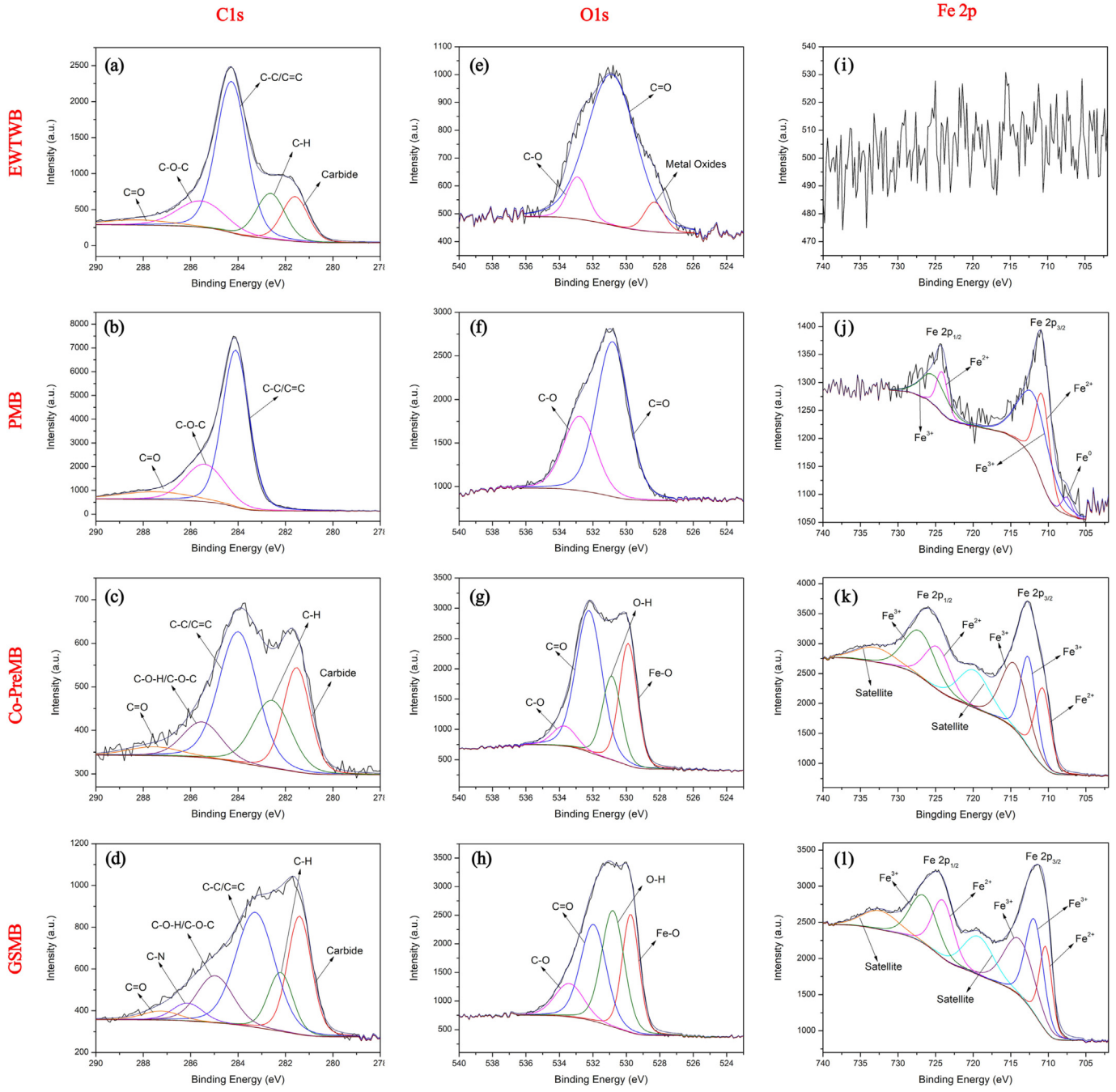


**Fig. 4.** Deconvolution of C1s, O1s and Fe2p of the biochars.

### *3.6. Stability of the adsorbents prepared*

To evaluate the stability of magnetic biochar, the leaching of irons from PMB, Co-PreMB and GSMB at pH range of 2 to 6 was investigated. As shown in Fig. S4, the leaching of iron followed identical pattern with rapid loss from pH 2 to pH 3, then the loss was negligible beyond pH 3 for both Co-PreMB and GSMB. At pH 2.0, the amount of iron released from Co-PreMB was 3.74 mg/g, and 6.62 mg/g for GSMB. The higher leaching amount in GSMB than Co-PreMB can be explained by the lower content of iron in Co-PreMB, and relatively poor bond between iron oxides and biochar in GSMB. There still was around 0.5 mg/g iron released from GSMB at pH 3 while Co-PreMB lost <0.1 mg/g iron at same condition. Therefore, Co-PreMB is comparably more stable than GSMB in acidic condition, and the pH range of application for Co-PreMB and GSMB is pH $\geq$3 and pH $\geq$ 4, respectively. For PMB, very less of iron was released into solution at the whole range of pH due to its low content of iron.

### *3.7. Plausible synthesis mechanism of GSMB*

The mechanism behind plant extract mediated metallic nanoparticle formation has not been clearly defined. Not a single biomolecule of plant extract was involved in the fabrication of nanoparticles, and these biomolecule can reduce $Fe^{3+}$ into $Fe^{2+}$ or ZVI. For tea extract, the polyphenols/caffeine play the key role in the formation of Fe/FeONPs (Karade et al., 2017). The higher activity agent concentration in the extract, the better stability and smaller particle size may result in higher reactivity of the FeNPs. The main phenolic compounds present in tea leaves are catechins and their derivatives, which constitute up to 30 % of their dry weight

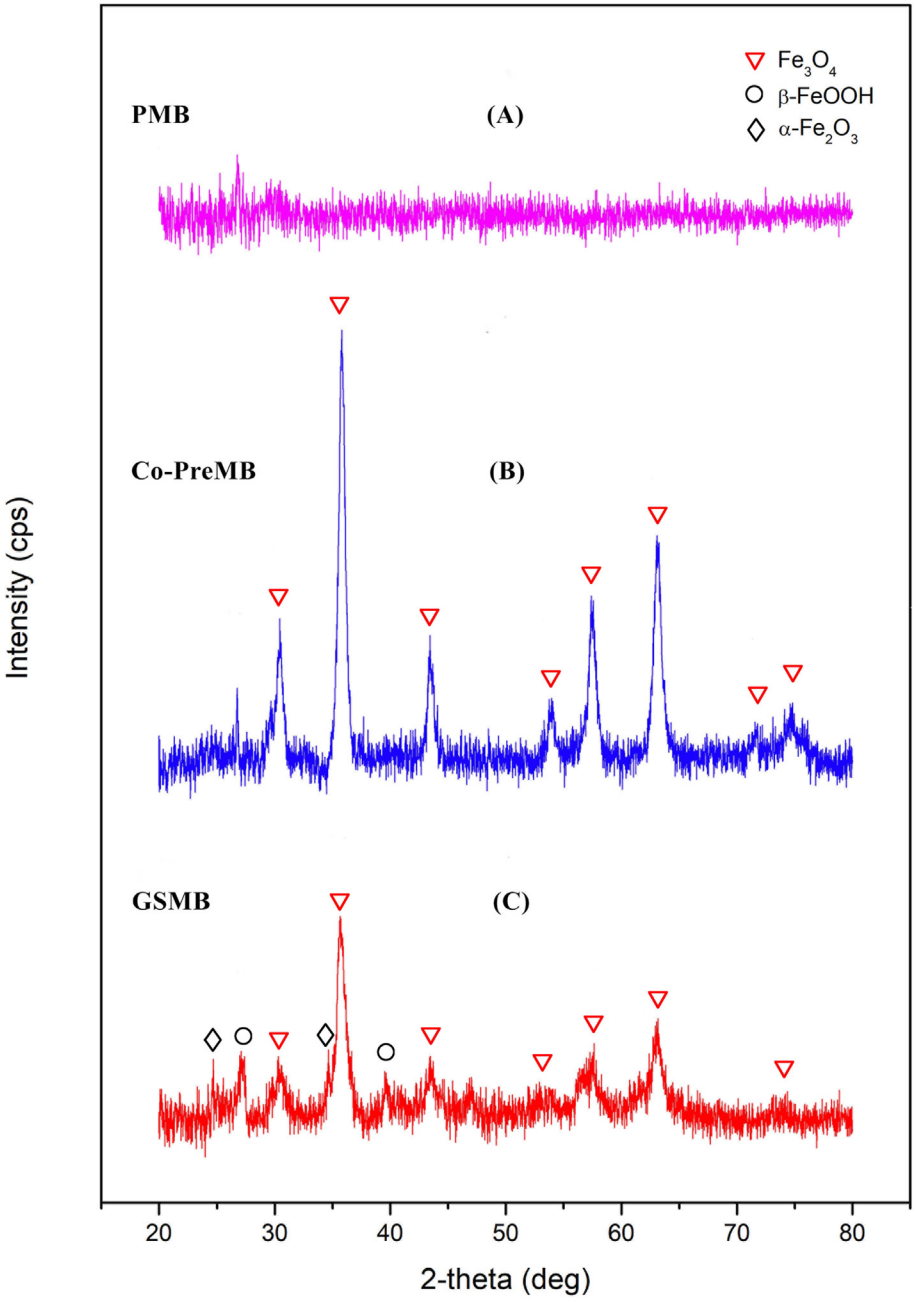


**Fig. 5.** XRD spectra of PMB (A), Co-PreMB (B) and GSMB (C).

(Dias et al., 2015). The main catechins present in white tea are shown in Fig. S5, and the synthesis of the $Fe_3O_4$ on the biochar can be divided into two stages which is shown in Fig. 6.

In the first step, the adjacent hydroxyl groups in catechin can act as chelation sites with $Fe^{3+}$ to form complexes and produce free radicals (Bernatoniene and Kopustinskiene, 2018). Then the $Fe^{3+}$ is reduced to $Fe^{2+}$ and the catechin is oxidized to the corresponding quinone either products directly or through the production of a secondary semi-quinone (Oakes and Oakes, 2013). Every adjacent hydroxyl groups can produce up to $2Fe^{2+}$ per reaction, therefore, the number of hydroxyl groups in the molecule correlates positively with the antioxidant activity of phenolic compounds (Rice-evans et al., 1995).

The second stage was a typical chemical co-precipitation of $Fe^{2+}$ and $Fe^{3+}$ in NaOH solution. The formation of $Fe_3O_4$ NPs occurs while further biological reduction of $Fe^{3+}$ takes place. Then along with the growth development, NPs tend to form a specific morphologies which determined by many factors such as the concentration of tea extract and precursor types (Njagi et al., 2011). The growth stage results in an enhancement of thermodynamic permanence of metal NPs while the stretched nucleation could result in accumulation of synthesized NPs. The whole reaction is terminated when the NPs achieve their maximum activity possible and the morphology keeps constant with the coverage of organic matters from the extract (Chokkareddy and Redhi, 2018).

## 4. Conclusions

Through this study we demonstrated the preparation of a novel biochar-based magnetic nanocomposites via green synthesis method by using white tea waste extract. Following conclusions were drawn from the study:

- Different physical and chemical characterizations such as SEM and XRD demonstrated the green synthesis method successfully introduced nano-sized $Fe_3O_4$ particles onto biochar.

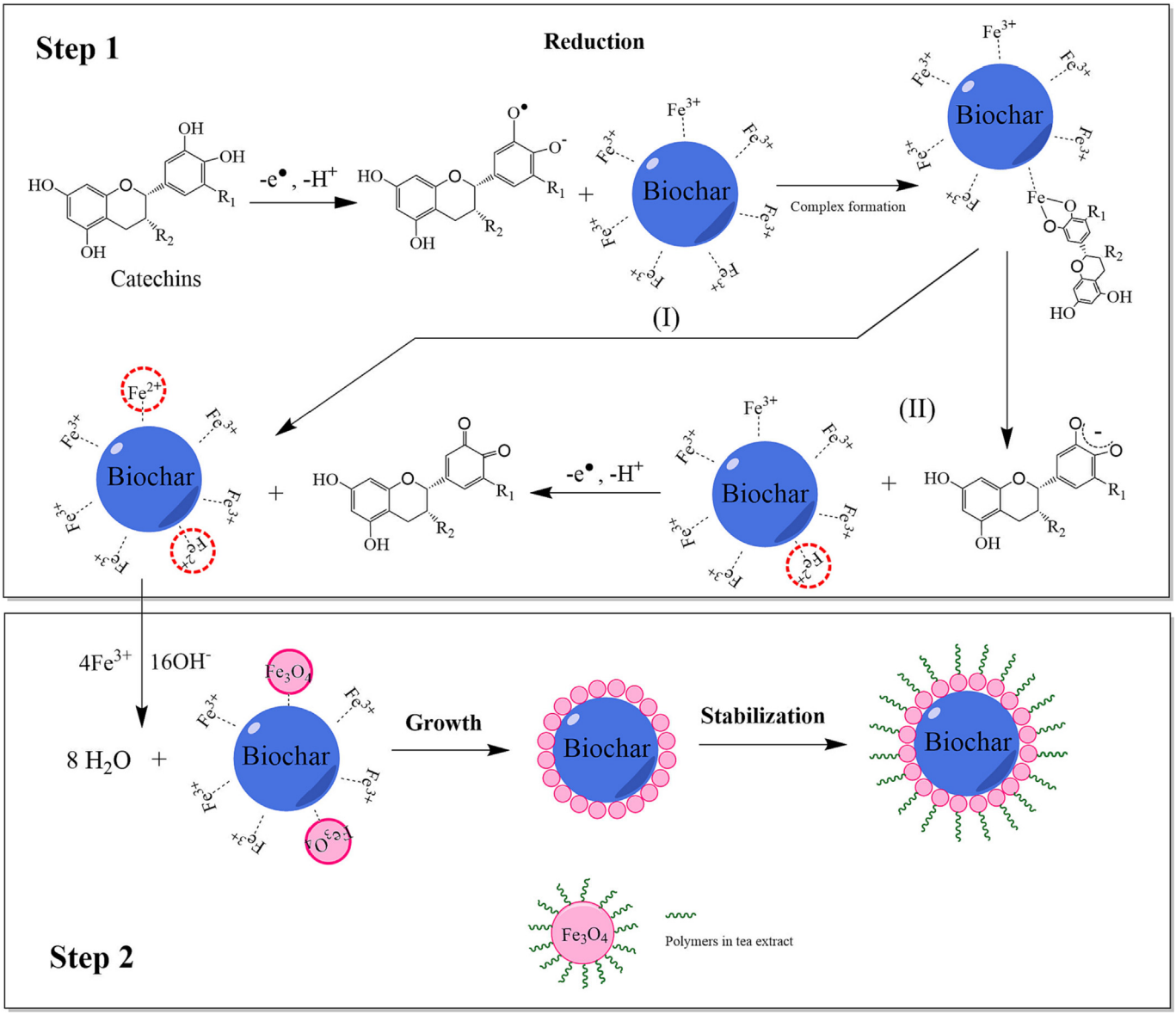


**Fig. 6.** A schematic representation of the mechanisms of introducing $Fe_3O_4$ nanoparticles onto biochar using white tea extract containing polyphenols like catechins.

- GSMB possessed the highest surface area and density of functional groups as compared to pristine biochar and other magnetic biochars produced in this study, indicating the great potential application of GSMB in wastewater treatment.
- However, GSMB is less stable in acidic conditions (pH < 4) than Co-PreMB and has lower saturation magnetization.

## CRediT authorship contribution statement

**Na Zhang:** Conceptualization, Investigation, Visualization, Writing - original draft.

**Febelyn Reguyal:** Review & editing.

**Sai Praneeth:** Sample characterisation and investigation

**Ajit K Sarmah:** Conceptualization, Validation, Supervision, Writing – review & editing, Funding acquisition and Correspondence.

## Data availability

The authors do not have permission to share data.

## Declaration of competing interest

All authors agree to their participation in this manuscript preparation and All authors also disclose that there is no financial and personal relationships with other people or organizations and no conflict of interest amongst the authors or organisations involved in this manuscript.

## Appendix A. Supplementary data

Supplementary data to this article can be found online at https://doi.org/10.1016/j.scitotenv.2023.163923.

## References

Bernatoniene, J., Kopustinskiene, D.M., 2018. The role of catechins in cellular responses to oxidative stress. Molecules 23, 1–11. https://doi.org/10.3390/molecules23040965.

Chen, X., Gao, X., Wu, H., 2022. Characterization of ashes from co-firing biochar with coal under pulverized-fuel conditions. ACS Eng. Au 2, 397–405. https://doi.org/10.1021/acsengineeringau.2c00012.

Chokkareddy, R., Redhi, G.G., 2018. Green synthesis of metal nanoparticles and its reaction mechanisms. Green Metal Nanopart., 113–139 https://doi.org/10.1002/9781119418900.ch4.

Chowdhury, Anurag, Sarkar, S., Chowdhury, Akash, Bardhan, S., Mandal, P., Chowdhury, M., 2016. Tea waste management: a case study from West Bengal,India. Indian J. Sci. Technol. 9, 1–6. https://doi.org/10.17485/ijst/2016/v9i42/89790.

Dias, T.R., Tomás, G., Teixeira, N.F., Alves, M.G., Oliveira, P.F., Silva, B.M., 2015. White tea (Camellia sinensis (L.)): antioxidant properties and beneficial health effects. Int. J. Food Sci. Nutr. Diet. 04, 1–5. https://doi.org/10.19070/2326-3350-130005.

Essandoh, M., Wolgemuth, D., Pittman, C.U., Mohan, D., Mlsna, T., 2017. Adsorption of metribuzin from aqueous solution using magnetic and nonmagnetic sustainable low-cost biochar adsorbents. Environ. Sci. Pollut. Res. 24, 4577–4590. https://doi.org/10.1007/s11356-016-8188-6.

Guo, S., Kumar Awasthi, M., Wang, Y., Xu, P., 2021. Current understanding in conversion and application of tea waste biomass: a review. Bioresour. Technol. 338, 125530. https://doi.org/10.1016/j.biortech.2021.125530.

Hu, X., Ding, Z., Zimmerman, A.R., Wang, S., Gao, B., 2015. Batch and column sorption of arsenic onto iron-impregnated biochar synthesized through hydrolysis. Water Res. 68, 206–216. https://doi.org/10.1016/j.watres.2014.10.009.

Huang, L., Weng, X., Chen, Z., Megharaj, M., Naidu, R., 2014. Green synthesis of iron nanoparticles by various tea extracts: comparative study of the reactivity. Spectrochim. Acta - Part A Mol.Biomol. Spectrosc. 130, 295–301. https://doi.org/10.1016/j.saa.2014.04.037.

Huang, X., Feng, B., Niu, Y., Zhao, L., Hu, W., 2018. Fenton-reaction-derived Fe/N-doped graphene with encapsulated Fe3C nanoparticles for efficient photo-Fenton catalysis. Catal. Lett. 148, 2528–2536. https://doi.org/10.1007/s10562-018-2425-1.

Hui, B.H., Salimi, M.N., 2020. Production of iron oxide nanoparticles by co-precipitation method with optimization studies of processing temperature, pH and stirring rate. IOP Conf. Ser. Mater. Sci. Eng. 743, 012036. https://doi.org/10.1088/1757-899X/743/1/012036.

Karade, V.C., Waifalkar, P.P., Dongle, T.D., Sahoo, S.C., Kollu, P., Patil, P.S., Patil, P.B., 2017. Greener synthesis of magnetite nanoparticles using green tea extract and their magnetic properties. Mater. Res. Express 4, 096102. https://doi.org/10.1088/2053-1591/aa892f.

Khan, F.S.A., Mubarak, N.M., Tan, Y.H., Karri, R.R., Khalid, M., Walvekar, R., Abdullah, E.C., Mazari, S.A., Nizamuddin, S., 2020. Magnetic nanoparticles incorporation into different substrates for dyes and heavy metals removal—areview. Environ. Sci. Pollut. Res. 27, 43526–43541. https://doi.org/10.1007/s11356-020-10482-z.

Kheshtzar, R., Berenjian, A., Taghizadeh, S.M., Ghasemi, Y., Asad, A.G., Ebrahiminezhad, A., 2019. Optimization of reaction parameters for the green synthesis of zero valent iron nanoparticles using pine tree needles. Green Process. Synth. 8, 846–855. https://doi.org/10.1515/gps-2019-0055.

Li, W., Yang, N., 2016. Green and facile synthesis of Ag–Fe3O4 nanocomposites using the aqueous extract of Crataegus pinnatifida leaves and their antibacterial performance. Mater. Lett. 162, 157–160. https://doi.org/10.1016/j.matlet.2015.09.064.

Lin, J., Weng, X., Dharmarajan, R., Chen, Z., 2017. Characterization and reactivity of iron based nanoparticles synthesized by tea extracts under various atmospheres. Chemosphere 169, 413–417. https://doi.org/10.1016/j.chemosphere.2016.11.092.

Liu, Y., Sohi, S.P., Liu, S., Guan, J., Zhou, J., Chen, J., 2019. Adsorption and reductive degradation of Cr(VI) and TCE by a simply synthesized zero valent iron magnetic biochar. J. Environ. Manag. 235, 276–281. https://doi.org/10.1016/j.jenvman.2019.01.045.

Mahdavi, M., Ahmad, M.Bin, Haron, M.J., Namvar, F., Nadi, B., Ab Rahman, M.Z., Amin, J., 2013. Synthesis, surface modification and characterisation of biocompatible magnetic iron oxide nanoparticles for biomedical applications. Molecules 18, 7533–7548. https://doi.org/10.3390/molecules18077533.

Maity, D., Kale, S.N., Kaul-Ghanekar, R., Xue, J.M., Ding, J., 2009. Studies of magnetite nanoparticles synthesized by thermal decomposition of iron (III) acetylacetonate in tri(ethylene glycol). J. Magn. Magn. Mater. 321, 3093–3098. https://doi.org/10.1016/j.jmmm.2009.05.020.

Makarov, V.V., Love, A.J., Sinitsyna, O.V., Makarova, S.S., Yaminsky, I.V., Taliansky, M.E., Kalinina, N.O., 2014. "Green" nanotechnologies: synthesis of metal nanoparticles using plants. Acta Nat. 6, 35–44. https://doi.org/10.1039/c1gc15386b.

Mohammadian, S., Krok, B., Fritzsche, A., Bianco, C., Tosco, T., Cagigal, E., Mata, B., Gonzalez, V., Diez-Ortiz, M., Ramos, V., Montalvo, D., Smolders, E., Sethi, R., Meckenstock, R.U., 2021. Field-scale demonstration of in situ immobilization of heavy metals by injecting iron oxide nanoparticle adsorption barriers in groundwater. J. Contam. Hydrol. 237, 103741. https://doi.org/10.1016/j.jconhyd.2020.103741.

Mohan, D., Kumar, H., Sarswat, A., Alexandre-Franco, M., Pittman, C.U., 2014. Cadmium and lead remediation using magnetic oak wood and oak bark fast pyrolysis bio-chars. Chem. Eng. J. 236, 513–528. https://doi.org/10.1016/j.cej.2013.09.057.

Mondal, P., Anweshan, A., Purkait, M.K., 2020. Green synthesis and environmental application of iron-based nanomaterials and nanocomposite: a review. Chemosphere 259, 127509. https://doi.org/10.1016/j.chemosphere.2020.127509.

Nassar, N.N., Arar, L.A., Marei, N.N., Abu Ghanim, M.M., Dwekat, M.S., Sawalha, S.H., 2014. Treatment of olive mill based wastewater by means of magnetic nanoparticles: decolourization, dephenolization and COD removal. Environ. Nanotechnol.Monit. Manag. 1–2, 14–23. https://doi.org/10.1016/j.enmm.2014.09.001.

Njagi, E.C., Huang, H., Stafford, L., Genuino, H., Galindo, H.M., Collins, J.B., Hoag, G.E., Suib, S.L., 2011. Biosynthesis of iron and silver nanoparticles at room temperature using aqueous sorghum bran extracts. Langmuir 27, 264–271. https://doi.org/10.1021/la103190n.

Oakes, Jacqueline S., Oakes, Jacqueline Shannon, 2013. Investigation of Iron Reduction by Green Tea Polyphenols for Application in Soil Remediation Application in Soil Remediation. Mater's Theses 528. https://opencommons.uconn.edu/gs_theses/528.

Pal, D., Maiti, S.K., 2019. Abatement of cadmium (Cd) contamination in sediment using tea waste biochar through meso-microcosm study. J. Clean. Prod. 212, 986–996. https://doi.org/10.1016/j.jclepro.2018.12.087.

Pariyar, P., Kumari, K., Jain, M.K., Jadhao, P.S., 2020. Evaluation of change in biochar properties derived from different feedstock and pyrolysis temperature for environmental and agricultural application. Sci. Total Environ. 713, 136433. https://doi.org/10.1016/j.scitotenv.2019.136433.

Parvathy, K.V.G., Krishna, S.M.M., Sudhahar, K.S., 2021. Celosia argentea leaf extract - mediated green synthesized iron oxide nanoparticles for bio - applications. J. Nanostruct. Chem., 1–16 https://doi.org/10.1007/s40097-021-00434-5.

Qiu, Y., Xu, X., Xu, Z., Liang, J., Yu, Y., Cao, X., 2020. Contribution of different iron species in the iron-biochar composites to sorption and degradation of two dyes with varying properties. Chem. Eng. J. 389, 124471. https://doi.org/10.1016/j.cej.2020.124471.

Rajapaksha, A.U., Vithanage, M., Zhang, M., Ahmad, M., Mohan, D., Chang, S.X., Ok, Y.S., 2014. Pyrolysis condition affected sulfamethazine sorption by tea waste biochars. Bioresour. Technol. 166, 303–308. https://doi.org/10.1016/j.biortech.2014.05.029.

Reddy, I.N., Sreedhar, A., Reddy, C.V., Shim, J., Cho, M., Kim, D., Gwag, J.S., Yoo, K., 2018. Enhanced visible-light photocatalytic performance of Fe3O4 nanopyramids for water splitting and dye degradation. J. Solid State Electrochem. 22, 3535–3546. https://doi.org/10.1007/s10008-018-4054-4.

Reguyal, F., Sarmah, A.K., 2018. Site energy distribution analysis and influence of Fe3O4 nanoparticles on sulfamethoxazole sorption in aqueous solution by magnetic pine sawdust biochar. Environ. Pollut. 233, 510–519. https://doi.org/10.1016/j.envpol.2017.09.076.

Rice-evans, C.A., Miller, N.J., Bolwell, P.G., Bramley, P.M., Pridham, J.B., 1995. The relative antioxidant activities of plant-derived polyphenolic flavonoids. Free Radic. Res. 22, 375–383. https://doi.org/10.3109/10715769509145649.

Shahwan, T., Abu Sirriah, S., Nairat, M., Boyaci, E., Eroğlu, A.E., Scott, T.B., Hallam, K.R., 2011. Green synthesis of iron nanoparticles and their application as a Fenton-like catalyst for the degradation of aqueous cationic and anionic dyes. Chem. Eng. J. 172, 258–266. https://doi.org/10.1016/j.cej.2011.05.103.

Shen, Y.F., Tang, J., Nie, Z.H., Wang, Y.D., Ren, Y., Zuo, L., 2009. Preparation and application of magnetic Fe3O4 nanoparticles for wastewater purification. Sep. Purif. Technol. 68, 312–319. https://doi.org/10.1016/j.seppur.2009.05.020.

Tan, X.fei, Liu, Y.guo, Gu, Y.ling, Xu, Y., Zeng, G.ming, Hu, X.jiang, Liu, Shao bo, Wang, X., Liu, Si mian, Li, J., 2016. Biochar-based nano-composites for the decontamination of wastewater: a review. Bioresour. Technol. 212, 318–333. https://doi.org/10.1016/j.biortech.2016.04.093.

Vinayagam, R., Zhou, C., Pai, S., Varadavenkatesan, T., Narasimhan, M.K., Narayanasamy, S., Selvaraj, R., 2021. Structural characterization of green synthesized magnetic mesoporous Fe3O4 NPs@ME. Mater. Chem. Phys. 262, 124323. https://doi.org/10.1016/j.matchemphys.2021.124323.

Wan, X., Li, C., Parikh, S.J., 2020. Simultaneous removal of arsenic, cadmium, and lead from soil by iron-modified magnetic biochar. Environ. Pollut. 261. https://doi.org/10.1016/j.envpol.2020.114157.

Wang, J., Zheng, S., Shao, Y., Liu, J., Xu, Z., Zhu, D., 2010. Amino-functionalized Fe3O4@SiO2 core-shell magnetic nanomaterial as a novel adsorbent for aqueous heavy metals removal. J. Colloid Interface Sci. 349, 293–299. https://doi.org/10.1016/j.jcis.2010.05.010.

Wang, T., Lin, J., Chen, Z., Megharaj, M., Naidu, R., 2014. Green synthesized iron nanoparticles by green tea and eucalyptus leaves extracts used for removal of nitrate in aqueous solution. J. Clean. Prod. 83, 413–419. https://doi.org/10.1016/j.jclepro.2014.07.006.

Wei, Y., Fang, Z., Zheng, L., Tsang, E.P., 2017. Biosynthesized iron nanoparticles in aqueous extracts of Eichhornia crassipes and its mechanism in the hexavalent chromium removal. Appl. Surf. Sci. 399, 322–329. https://doi.org/10.1016/j.apsusc.2016.12.090.

Xu, D., Cao, J., Li, Y., Howard, A., Yu, K., 2019. Effect of pyrolysis temperature on characteristics of biochars derived from different feedstocks: a case study on ammonium adsorption capacity. Waste Manag. 87, 652–660. https://doi.org/10.1016/j.wasman.2019.02.049.

Yamashita, T., Hayes, P., 2008. Analysis of XPS spectra of Fe2+ and Fe3+ ions in oxide materials. Appl. Surf. Sci. 254, 2441–2449. https://doi.org/10.1016/j.apsusc.2007.09.063.

Yang, J., Zhao, Y., Ma, S., Zhu, B., Zhang, J., Zheng, C., 2016. Mercury removal by magnetic biochar derived from simultaneous activation and magnetization of sawdust. Environ. Sci. Technol. 50, 12040–12047. https://doi.org/10.1021/acs.est.6b03743.

Yao, X., Ji, L., Guo, J., Ge, S., Lu, W., Cai, L., Wang, Y., Song, W., Zhang, H., 2020. Magnetic activated biochar nanocomposites derived from wakame and its application in methylene blue adsorption. Bioresour. Technol. 302, 122842. https://doi.org/10.1016/j.biortech.2020.122842.

Yuan, J.H., Xu, R.K., Zhang, H., 2011. The forms of alkalis in the biochar produced from crop residues at different temperatures. Bioresour. Technol. 102, 3488–3497. https://doi.org/10.1016/j.biortech.2010.11.018.

Zhang, M., Gao, B., Varnoosfaderani, S., Hebard, A., Yao, Y., Inyang, M., 2013. Preparation and characterization of a novel magnetic biochar for arsenic removal. Bioresour. Technol. 130, 457–462. https://doi.org/10.1016/j.biortech.2012.11.132.

Zhao, Y., Zhang, R., Liu, H., Li, M., Chen, T., Chen, D., Zou, X., Frost, R.L., 2019. Green preparation of magnetic biochar for the effective accumulation of Pb(II): performance and mechanism. Chem. Eng. J. 375, 122011. https://doi.org/10.1016/j.cej.2019.122011.